https://doi.org/10.5194/egusphere-2025-6516
Preprint. Discussion started: 6 January 2026

Suspended sediment transport modulated by microbial activities in estuarine waters: Insights from molecular and structural perspectives

Yanjia Wang[1], Jie Ren[1*], Leiping Ye[1*], Jia-Ling Li[2,3], Yaokun Lin[1,2], Lei Zhang[4], Ya Wu[1], Wen-Jun Li[3], Jiaxue Wu[1]

[1]School of Marine Sciences, Sun Yat-sen University, Southern Marine Science and Engineering Guangdong Laboratory (Zhuhai), Zhuhai, Guangdong 519082, China.
[2]Southern Marine Science and Engineering Guangdong Laboratory (Guangzhou), Guangzhou, Guangdong 511458, China.
[3]School of Life Sciences, Sun Yat-Sen University, Guangzhou, 510275, China.
[4]Guangdong Provincial Key Laboratory of Applied Botany, South China Botanical Garden, Chinese Academy of Sciences, Guangzhou 510650, China.
*Corresponding authors: Leiping Ye (yeleiping@mail.sysu.edu.cn) and Jie Ren (renjie@mail.sysu.edu.cn)

https://doi.org/10.5194/egusphere-2025-6516
Preprint. Discussion started: 6 January 2026

Abstract

Suspended sediment transport in coastal estuaries is profoundly shaped by microbial activities, yet the underlying molecular mechanisms remain poorly constrained during their flocculation. Here, we demonstrate that the estuarine bacterium *Stutzerimonas decontaminans* acts as a key mediator of sediment flocculation. Compared to purely physical aggregation, microbially-induced flocculation developed more slowly but yielded flocs fourfold larger, with looser fractal structures and higher organic carbon content, indicating strong microbial-mineral coupling. Bacteria modulated flocculation both physically via flagella-driven adhesion and biochemically through extracellular polymeric substances, which enhanced particulate organic carbon accumulation. Transcriptomic analyses revealed an early upregulation of flagellar genes initiating particle adhesion, followed by the activation of polysaccharide biosynthesis pathways to stabilize aggregates. This sequential regulation highlights a genetic trade-off between motility and biofilm-like stickiness in controlling floc growth. Our findings provide direct molecular and structural evidence that microbial activities fundamentally reshape sediment aggregation dynamics, thereby regulating suspended sediment transport and carbon cycling in coastal systems.

Key words: Bio-flocculation, microorganisms, extracellular polymeric substances (EPS), floc structure, gene regulation, estuary.

https://doi.org/10.5194/egusphere-2025-6516
Preprint. Discussion started: 6 January 2026

1. Introduction

Estuaries, as critical ecological transition zones between land and ocean, play a central role in global biogeochemical cycles (Gattuso et al., 1998; Burchard et al., 2018). As hubs for land-derived materials and carbon cycling, the formation, growth, breakup, and settling of mud flocs exert fundamental controls on suspended sediment transport (Zhu et al., 2021), the fate of particulate organic carbon (POC) (Bauer et al., 2013), the transformation of pollutants (Li et al., 2023), and the cycling of biogeochemical elements (Turner & Millward, 2002).

Previous studies on mud flocculation dynamics mostly focused on physicochemical factors such as flow shear, salinity-induced charge neutralization, and particle concentration and composition (e.g., Mietta et al., 2009; Moruzzi et al., 2017; Tran et al., 2018; Guo et al., 2021; Ye et al., 2023). However, growing evidence indicates that purely physicochemical models cannot fully explain the developmental behaviors of natural suspended mud flocs. Particle-associated microbial processes have gradually been incorporated into conceptual and numerical models (e.g., Maggi, 2009; Lai et al., 2018; Nguyen et al., 2018; Shen et al., 2019), thereby extending traditional flocculation theory. Moreover, bioflocculation dynamics exert strong influence on estuarine-coastal material or elements cycling (e.g., Droppo, 2001; Nguyen et al., 2022) and thus provide key scientific guidance for estuarine dredging, channel maintenance, water quality management and estuarine restoration globally (Cox et al., 2022; Chen et al., 2024).

Bio-flocculation, driven by active microorganisms (bacteria, algae, viruses, fungi, protozoa, etc.), has been recognized as a central engine controlling the aggregation, transformation, and transport of suspended sediments in estuaries (Burd & Jackson, 2009; Dang & Lovell, 2016; Deng et al., 2022). Compared with mineral clay particles aggregation chemically, mud flocculation processes highly mediated by natural estuarine microbial strains, algae, fungus, and bacterial extracellular polymeric substances (EPS) profoundly alter surface physicochemical properties and structures, significantly affecting floc size, density, and porosity (e.g., Tang & Maggi, 2016; Deng et al., 2023; Ho et al., 2022; Nguyen et al., 2017; Labille et al., 2005; Ye et al., 2023). This produces bio-mineral aggregates that are larger, more porous, and structurally more complex than mineral-only flocs, thereby modifying settling velocities, transport dynamics, and adsorption behaviors (Passow & De La Rocha, 2006; Chapalain et al.,

https://doi.org/10.5194/egusphere-2025-6516
Preprint. Discussion started: 6 January 2026

2019). Bio-flocculation is inherently dynamic, and we hypothesize that bio–mineral mixed flocs under continuous shear forces reach a state of dynamic balance between aggregation and breakup. Yet, the molecular mechanisms by which marine microorganisms perceive environmental signals and regulate the formation, structural evolution, and transport behavior of suspended flocs remain poorly understood (Belas, 2014; Dang & Lovell, 2016; Berne et al., 2018; Sun & Zhang, 2021).

The molecular basis of bacterial colonization and EPS secretion, and their functional roles in bio-flocculation and sediment transport, remain insufficiently studied, especially in complex estuarine and marine systems. In recent years, high-throughput sequencing technologies such as transcriptomics have provided powerful tools to resolve EPS bio-synthetic pathways (e.g., Schmid et al., 2015; Shukla et al., 2019; Rana & Upadhyay, 2020; Sun & Zhang, 2021; He et al., 2024). Here, we investigate how dominant EPS-producing estuarine bacteria (e.g., *Stutzerimonas decontamans*) (Wu et al., 2017; Mulet et al., 2023) influence the flocculation of inorganic clay minerals (e.g., montmorillonite) under high turbulent shear. Specifically, this study addresses following key questions: Compared with inorganic mineral flocculation, how do prokaryotes and their EPS regulate the kinetics and structural characteristics of bio-mineral suspended flocs? How do microbial processes modulate environmental factors during flocculation? What are the key gene expression patterns and molecular regulatory mechanisms underlying bio-flocculation? To this end, we conducted series bacterial-mineral flocculation experiments using a custom-designed reaction system. By coupling AI-based image analysis with transcriptomic approaches, new insights into the dynamic processes and molecular mechanisms through which microbial activity modulates suspended sediment transport in estuaries have been provided.

2. Materials and Methods

2.1. Laboratory experimental setup

A self-designed Experimental Facility for Sediment Bio-flocculation (EFSB; Fig.1) equipped with a unified camera system has been used in this study. Each experiment comprised at least three replicate apparatuses to ensure reproducibility. The mixing chamber served as the core site for bacterial growth and bio-flocculation, and therefore underwent strict sterilization. A stainless-steel shaft (30 cm) with a 12 cm three-bladed

https://doi.org/10.5194/egusphere-2025-6516
Preprint. Discussion started: 6 January 2026

propeller was inserted into the chamber containing 5 L salt-supplemented medium. The chamber was sealed with a custom quartz plate (φ 20 cm) and a red rubber O-ring; the shaft tip passed precisely through the plate's central bore (φ 15 mm). The assembly was wrapped with plastic film and autoclaved at 121 °C for 15 min (GI80, Zealway). After cooling to room temperature, the chamber was mounted on the bench base, the stirrer was connected to a variable-speed drive, and the system was brought to a constant rotational speed of 100 rpm, corresponding to a shear rate of 65 s^{-1} pre-calibrated in a 5 L sediment suspension using an Acoustic Doppler Velocimeter (ADV; Nortek).

For on-line sampling and imaging, a peristaltic pump set to 40 mL min^{-1} drove the suspension through a sampling assembly comprising a 25 cm glass tube (ID 5 mm), a square quartz tube (length 10 cm; ID 3 mm; wall 0.5 mm), and two rubber connectors (ID 3.2 mm). As flocs traversed the square quartz tube, the "shooting point", focal distance 3.5 cm, they were recorded by a high-speed camera (AcutEye-1M-2000) with a 300 W LED light source synchronized to a computer. After each sampling, an equal volume of fresh sterile medium was replenished via a sterile line using an electronic pipette (Model S1, Thermo Fisher Scientific) to maintain a constant shear history.

2.2. Experimental treatments

Bio-flocculation processes were investigated in systems containing montmorillonite clay and *Stutzerimonas decontaminans* (hereafter *S. decontaminans*), a dominant bacterium in the Pearl River Estuary known for high EPS production (Li et al., 2018). Montmorillonite (High-Purity Clay Mineral Repository of China) had a median particle size D_{50} of 13.30 μm (Mastersizer 3000, Malvern Panalytical, UK). Three experimental series were established:

(1) **SD (pure biological material)**: *S. decontaminans* was inoculated into 5 L basal salt medium (1.2 $g \cdot L^{-1}$ R2A nutrients + 15 $g \cdot L^{-1}$ NaCl) and cultured at room temperature for 72 h under high shear (65 s^{-1}).

(2) **MM (montmorillonite only)**: 10 mL mineral stock (50 $g \cdot L^{-1}$) was added to 5 L saline (15 PSU) and vigorously mixed at 300 rpm for 5 min to form initial flocculi, followed by 160 min at constant G = 65 s^{-1}.

(3) **MSD (bio-material and mineral mixture)**: A 12-h culture of *S. decontaminans* was combined aseptically with 10 mL sterilized mineral stock (50 $g \cdot L^{-1}$) and maintained for 48 h at G = 65 s^{-1}. Continuous turbulent mixing (G = 65 s^{-1})

https://doi.org/10.5194/egusphere-2025-6516
Preprint. Discussion started: 6 January 2026

minimized aggregation-driven settling. Replicates were n = 6 for MSD and n = 3 for MM and SD.

2.3. Image processing and floc structures

Sampling protocols differed between the MM and MSD. Specifically, the MM treatments were sampled every 20 minutes, whereas the MSD treatments were sampled initially every 3 hours (12-24 h) and then every 6 hours until 48 h (Fig.2a). At each imaging time point, flocs at the shooting point were recorded at 20 Hz for 2-3 min (~3000 frames per time) (Fig.2b). Images were curated and processed in Python 3.10 using an instance-segmentation workflow based on YOLOv8-seg (Fig.2d) (Jocher et, al., 2023), including preprocessing and standardization, object detection and instance segmentation with an improved YOLOv8-seg (confidence threshold 0.6 and size filters), contour refinement via Gaussian smoothing and morphological opening, morphological feature extraction, and secondary filtering and statistics.

Projected area (A), perimeter (L), ratios of major/minor axes, and related metrics were derived from segmented masks. The sphere-equivalent diameter was computed as $D_{eq}=2A/\pi$ after converting pixels to physical units (1 pixel = 1.8 μm). The two-dimensional fractal dimension N_f was estimated from perimeter-area scaling (i.e., $L \propto A \cdot N_f/2$) (Moruzzi et, al., 2017). Particle-size distributions (PSD) were constructed in 5 μm bins; D_{50} and D_{90} were reported. Flocs were also grouped into size classes of 0-20 μm, 20-60 μm, 60-120 μm, and >120 μm to compare MM and MSD dynamics.

2.4. Microstructural characterization for particles (SEM and AFM)

Mixed flocs (MSD) and mineral flocs (MM) were immobilized on ITO-coated conductive glass slides (20×10×1.1 mm; GOLO, China). Samples of MSD were equilibrated in phosphate buffer (pH 7.0), fixed with 2.5 % glutaraldehyde at 4 °C for ≥ 4 h, dehydrated through graded ethanol (30-100 %, 15 min per step), and air-dried (Anvari-Yazdi et, al., 2014). For **scanning electron microscopy (SEM)**, specimens were sputter-coated with Au–Pd and imaged (Axia ChemisEM HiVac, Thermo Scientific). Elemental mapping via SEM was used to revealed the elemental composition of these flocs. For **atomic force microscopy (AFM)**, dried samples were scanned (Dimension FastScan, Bruker) to obtain 3-D topography and surface potential;

https://doi.org/10.5194/egusphere-2025-6516
Preprint. Discussion started: 6 January 2026

NanoScope Analysis (v1.9) with third-order flattening provided surface roughness parameters (Ra, Rq) and potential distributions.

2.5. Laboratory sampling and physicochemical measurements

In MSD, imaging and sample collection were synchronized (Fig.2b-c). For transcriptomics, three biological replicates (100 mL each) were filtered onto 0.22 μm membranes (Pall Life Sciences, USA), flash-frozen in liquid N_2, and stored at -80 ℃ until RNA extraction. An additional 100 mL aliquot was used for biochemical and microbial indicators: 10 mL through a 0.22 μm GF/F filter (Whatman International Ltd., England) for particulate organic carbon (POC), and 20 mL through a sterile 0.22 μm membrane (Pall Life Sciences, USA) for 16S rRNA quantification; membranes were stored at -20 ℃. Filtrates were used for (1) dissolved organic carbon (DOC; 10 mL), (2) EPS extraction by adding three volumes of absolute ethanol to 10 mL filtrate, and (3) dissolved inorganic nitrogen (NO_x = NO_2^- + NO_3^- + NH_4^+; 15 mL). Filtrates were stored at 4 ℃ until analysis.

POC and DOC were measured by combustion oxidation with non-dispersive IR detection (TOC-VCPN, Shimadzu, Japan). Proteins were quantified by the Lowry assay （BSA standard; 490 nm; Lowry et al., 1951) and polysaccharides by the phenol–sulfuric acid method (glucose standard; 750 nm; DuBois et al., 1956) on a microplate reader (Multiskan Sky, Thermo Fisher Scientific, USA). Total EPS was calculated as protein + polysaccharide. NH_4^+-N, NO_2^--N, and NO_3^--N were measured with a continuous-flow analyzer (QuAAtro 39, Seal Analytical, UK) and summed as NO_x. pH and zeta potential were determined on 15 mL subsamples using a pH meter and a BeNano 90 Zeta analyzer (Dandong Better Instruments, China), respectively; turbidity was measured on the remaining suspension (2100N, HACH, USA).

2.6. Bacterial Growth Curves

Both SD and MSD treatments were sampled every 3 hours from 12 to 24 h, followed by 6-hour-interval sampling until 72 h (SD) and 48 h (MSD), respectively (Fig.2a). All microbial samples were immediately filtered for DNA extraction. After assessing the DNA concentration and integrity of all samples using a Qubit 3.0 fluorometer and agarose electrophoresis, a mixture of synthetic spike-in standards at graded concentrations was added to each DNA pool. The V4-V5 region of the 16S

https://doi.org/10.5194/egusphere-2025-6516
Preprint. Discussion started: 6 January 2026

rRNA gene and spike-in sequences were amplified with primers 515F and 907R and sequenced on an Illumina NovaSeq 6000 (Tkacz et, al., 2018). Absolute quantification based on spike-in calibration was performed by Genesky Biotechnologies (Shanghai, China). The data obtained from viable DNA quantification were used to generate the bacterial growth curves. The following experiments were conducted during the logarithmic phase of growth in MSD.

2.7. Transcriptomic analysis

To elucidate the differential expression and transcription of genes that regulate the flocculation process. Total RNA was extracted using the Soil RNA Extraction Kit (RNS485) (Mei5 Biotechnology Co., Ltd, China). RNA sequencing and analysis were carried out by Guangdong Magigene Technology Co., Ltd (Guangzhou, China) (Callahan et, al., 2016; Guo et, al., 2024).

Quality control was conducted on both the genome and transcriptome data, followed by genome assembly and subsequent annotation using the cleaned data. To analyze the gene expression abundance, sequencing reads were used to perform alignment using Bowtie2. Gene expression was quantified using FPKM (Fragments Per Kilobase per Million mapped reads). Differentially expressed genes (DEGs) were identified with a threshold of false discovery rate (FDR) ≤ 0.05 and $|\log_2(\text{fold change})| \geq 1$. Finally, all FPKM values were $\log_2$-transformed for subsequent downstream analyses. Selected genes encompassed core components of global regulators (e.g., *PhoQ, RpoS, RcsC*), c-di-GMP metabolism (e.g., *PleD*), flagellar assembly (e.g., *flg, fli, motA/B*), polysaccharide synthesis (e.g., *galE, glk, epsL*). Information of key enzymes in the synthesis of EPS used in this study was shown in Table S1.

2.8. Statistical analysis

One-way ANOVA was used to test temporal differences in mean diameter (D_m), D_{50}, D_{90}, and N_f between MSD and MM. Temporal trends in bacterial growth, genes exhibiting expression, and physicochemical variables were analyzed similarly. When ANOVA indicated significance ($P < 0.05$), Tukey's HSD was applied for pairwise comparisons. Principal component analysis (PCA) was used to assess overall transcriptional shifts across different stages. Analyses and plots were produced in Origin 2024. Partial least-squares path modeling (PLS-PM) was used to evaluate direct

https://doi.org/10.5194/egusphere-2025-6516
Preprint. Discussion started: 6 January 2026

and indirect effects of *S. decontaminans* (flagellar motility/polysaccharide synthesis) on inorganic flocculation; models were built with the plspm package in R4.2.2.

3. Results

3.1. Microbial role on mud flocculation enhancement

The mineral-only system (MM) reached equilibrium rapidly according to the experimental results, in one hour (Fig.3a-d), with a resulting equilibrium diameter (D_m) of approximately 30 μm and a steady N_f value of 1.54 (Fig. 3a-d). As shown in Fig.1e, a predominance of small particles (20–60 μm, 68.92%) was observed in the MM with the maximum D_{90} of 49 μm. Larger aggregates (>60 μm) were scarce and remained below 5.5 % of total abundance (Fig.3e).

In contrast, the bio-mineral system (MSD) underwent a prolonged three-stage trajectory spanning 12-48 h (Fig.3g-i), characterized by rapid growth (12-18 h) (Fig.3g), decelerated aggregation (21-30 h) (Fig.3h), and dynamic equilibrium (36-48 h) (Fig.3i). Even after the mean floc sizes (D_m=113 μm) stabilized, D_{90} continued to increase (Fig.3d), a trend driven by the growing proportion of large flocs (> 120 μm; 37.03%) (Fig.3f), indicating a persistent capacity for large floc formation. At equilibrium, MSD produced aggregates 3.8 times larger than MM, with fractal dimensions consistently lower (1.43), reflecting looser and more open structures (Fig.3b).

3.2. Structural re-organization and self-adaption of mud flocs

Beyond enhancing floc size, microorganisms restructured aggregate architecture at the microscale (Fig.4). SEM imaging clearly revealed that MSD flocs developed irregular, loosely bound morphologies, in contrast to the compact aggregates in MM (Fig.4a-d). Moreover, evidence of bacterial and EPS matrix binding to mineral grains was observed in Fig.4b,c,e,f.

As a key component of flocs, EPS, was observed to form a distinct structural entity, exhibiting a fibrous or ribbon-like morphology (Fig.4e, Fig.5d), which contributed to enhanced toughness and structural stability for mixed flocs.

The elemental composition confirmed microbial contributions to the mixed flocs, marked by significant carbon (C, 7.4%) and predominant oxygen (O, 70.4%) contents (Fig.5a-c)— both values closely aligned with those in a EPS dominant sample (C, 8.2%; O, 77.4%; Fig.5 d-f). Alongside this biological signature, the dominant mineral

https://doi.org/10.5194/egusphere-2025-6516
Preprint. Discussion started: 6 January 2026

composition was characterized by silicon (Si, 13.3%) and aluminum (Al, 3.5%) in the mixed flocs. In contrast to the patterns described above, we also observed that the carbon-dominated particles (53.9%) exhibited lower oxygen levels (32.3%) and, correspondingly, a smaller structural size (Fig.5g-i).

AFM analysis provides quantitative evidence for these structural modifications (Fig.6a-b). Mineral surfaces exhibited greater roughness (R_q = 66.6 nm) and higher surface potentials (232 mV) than bacterial surfaces (R_q = 32.9 nm; 137 mV) (Fig.6a-b). When combined, these contrasts reduced the effective electrostatic barrier. Zeta potential measurements corroborated this effect: Absolute potentials were highest in MM, followed by MSD and SD, with MSD displaying a marked decline as bacterial growth (Fig.6c-d).

3.3. Microbial abundance, EPS, and physicochemical parameters

Under pure culture conditions, *S. decontaminans* entered the logarithmic growth phase after 9 h post-inoculation and reached its peak density at 36 h, with a maximum bacterial abundance of 2.05×10^7 copies/mL (Fig.7a). The population subsequently entered the stationary phase between 42 and 72 hours, maintaining a stable abundance level of approximately 1.36×10^7 copies/mL.

In the MSD, the *S. decontaminans* population exhibited sustained logarithmic growth throughout the 12-48 h period, with abundance increased significantly from 2.99×10^5 copies/mL at 12 h to 2.43×10^7 copies/mL at 48 h. During this period, the total EPS content and its primary components (polysaccharides and proteins) showed no significant variations during the experimental period both in the MSD and SD (Fig.7b). Nevertheless, MSD exerted a significant influence on other environmental factors. Specifically, the POC content in the MSD increased significantly after 30 h, accumulating to 29.18 mg/L at 48 h (Fig.7c).

Concurrently, both DOC and NO_x exhibited significant decreasing trends throughout the experimental period (Fig.7d-e). Besides, the accumulation of organic matter in the MSD led to a significant increase in turbidity along with a pronounced decrease in pH (Fig.7f-h).

3.4. Biological molecular regulation of mud flocculation dynamics

Once the dynamics and structures of biophysical flocs can be affected by microbial

https://doi.org/10.5194/egusphere-2025-6516
Preprint. Discussion started: 6 January 2026

activity (Fig.3, Fig.4 and Fig.7a), we sought to delineate underlying changes in the gene transcriptome that may account for mud flocculation behavior. For this purpose, we investigated genes essential for EPS regulation, with a focus on the global regulatory system, flagellar system, and polysaccharide biosynthesis pathways (Fig.8, Tables S1-S4). Among the about 40 genes surveyed, over three-quarters showed differential expression during the 12-48 h experimental period (Tables S2-S4). To gain further insight into how genes regulate flocculation, we employed principal component analysis (PCA) to assess overall transcriptional shifts across different flocculation stages (Fig.9), and then identified the regulatory patterns of stage, specific differentially expressed genes (Fig.10).

The results from PCA analysis confirmed stage-specific transcriptional shifts throughout flocculation. The first two principal components (PC1 and PC2) captured 52.40% and 16.20% of the total transcriptional variance (68.6%), respectively. As illustrated in Fig. 9, the distinct separation along PC1 revealed that time-dependent changes dominate the transcriptional profile, driving a continuum from motility and early attachment (Stage 1) through metabolic adaptation (Stage 2) to stable matrix assembly (Stage 3). Notably, polysaccharide synthesis genes and flagellar genes exhibited an inverse distribution along the PC2 axis, reflecting an underlying biological trade-off between motility and EPS production.

In the early phase (12-15 h) of Stage one, flagellar structural and motor genes (e.g., *flgE/F/G/H/I/L, fliP/F/G/I/D, motA/B*) were upregulated (Table S3), corresponding to a burst of motility-driven adhesion that triggered a rapid rise in floc size. Finishing initial colonization, the cells gradually downregulated flagellar structural (Fig.10a) while upregulating genes involved in the metabolism of specific carbon sources (such as maltose, e.g., *malE/P/Q/S*), thereby storing energy and precursor substances (*glk, rmlC/D*) for the EPS production in Stage two (Fig. 10b, Tables S4). Compared to Stage one, the expressi on of *rpoN* was notably downregulated, while *rpoS* was significantly upregulated in Stage two (Fig.9a-b), acting in concert to regulate the shift in bacterial behavior from motility to adherence.

In Stage three, the stability of the floc structure was determined by both the low expression of flagella-related genes and the stable expression of EPS synthesis pathway. Specifically, the reduced expression of genes associated with flagellar structure (e.g., *flg, fli*) and motility (*mot*) facilitated floc stabilization (Fig.10a, Tables S3). Although

https://doi.org/10.5194/egusphere-2025-6516
Preprint. Discussion started: 6 January 2026

the downregulation observed in one EPS-related pathways such as *pleD, glmM, epsL,* the steady state of the expression of genes, eg., two-component signaling (*rcsC*), sigma factor(*rpoS*) and polysaccharide synthesis (*glk, rmlC/D, galE*) (Fig.10b, Tables S2,4) served as a major driver for floc stability.

3.5. Effects of microorganisms

Microbes not only restructure aggregates but also couple sediment dynamics to carbon cycling. A PLS-PM analysis (GOF = 0.70) showed that bacteria production promoted POC accumulation, while DOC declined in parallel (Fig.11). Ultimately, however, this pathway exerted a net inhibitory effect on floc formation (path coefficient = -1.03; Fig.11). Also, path analysis confirmed this negative effect, with flagellar activity exerting a strong inhibitory influence on floc structure (path coefficient = -0.96; Fig.11). In addition, microbial activity significantly affected environmental variables such as pH, turbidity, and nitrogen oxides (path coefficient = 0.62), though these parameters did not directly alter floc structure (Fig.11).

4. Discussion

Synthesizing these findings, we propose a three-stage conceptual framework (Fig. 12) to systematically elucidate the microbial-mediated dynamic restructuring and adaptive processes of flocs. The first stage initiates through flagella-mediated initial cellular adhesion; the second stage consolidates aggregates via EPS-mineral interactions; and the third stage enhances floc structural stability through polysaccharide biosynthesis. Traditional flocculation models emphasize the transient equilibrium governed by physicochemical factors, such as turbulence, ionic strength, and particle concentration (e.g., Winterwerp, 1998; Zhao et al., 2021; Cui et al., 2023), however these physicochemical approaches fail to explain the persistence of large, porous aggregates frequently observed in natural estuaries. Our controlled experiments demonstrate that microbial activity is essential to bridge this gap.

The ecological significance of microbial enhancement on mud flocculation is profound. In natural estuaries, bio-flocculation hardly proceeds to equilibrium due to turbulence and shear constantly disruptions. The slower but sustained growth of MSD suggests that bio-flocs can remain dynamic under fluctuating conditions, continually reaggregating and persisting in suspension (Fig.3b). This microbial extension of

https://doi.org/10.5194/egusphere-2025-6516
Preprint. Discussion started: 6 January 2026

flocculation timescales explains why field measurements consistently record larger, carbon-rich aggregates than predicted by mineral-only models (Fettweis et al., 2022; Deng et al., 2022; Nguyen et al., 2022; Baumas & Bizic, 2024). Microorganisms, therefore, provide a biological buffer that maintains suspended floc populations, modulating both sediment and organic matter transport.

The looser fractal structures (N_f=1.43) observed in MSD (Fig.3b) imply aggregates with lower effective density, higher porosity, and greater deformability under shear. Such characteristics directly influence transport behavior: bio-flocs with EPS are expected to settle more slowly, remain longer in suspension (Maggi, 2009, 2013), and be advected further downstream compared to denser mineral flocs (Zhu et al., 2021). These properties also enhance the capacity of flocs to trap and carry particulate organic matter, nutrients, and contaminants. Previous studies have hypothesized that EPS-rich flocs are critical carriers of carbon and pollutants, elements (e.g., Passow, 2002; Decho & Gutierrez, 2017; Mari et al., 2017; Baumas & Bizic, 2024), but here we provide direct imaging and electrochemical evidence of the mechanisms by which microbes reshape floc architecture to achieve these transport functions. Results of AFM and zeta potential demonstrated (Fig. 6) that the decreasing repulsion facilitated cohesion among particles and allowed EPS-mediated adhesion to dominate floc formation (Labille et al., 2005; Ye et al., 2023; Walshire et al., 2024). Moreover, organic matter contributed 7.4 % - 53.9 % of MSD composition (Fig.5), indicating that microbes not only accelerate aggregation but also fundamentally alter its biochemical composition.

Gene expression sequential regulatory program (Fig.8,9,10, Tables S1-4) explains the slower kinetics yet larger and looser outcomes of bio-flocculation compared with mineral flocculation. It also highlights a central microbial strategy: balancing dispersal and cohesion through stage-dependent gene expression. The molecular evidence thus provides a mechanistic basis for the structural transformations observed in Figure 10 and validates the pathway interactions revealed by the figure 11. This physiological shift represents a trade-off: initial motility enables contact (O'Toole et al., 1998; Belas, 2014; Berne et al., 2018; Wadhwa & Berg, 2022), but stability requires suppression of movement and investment in EPS production (Gerbersdorf & Wieprecht, 2015; Dar et al., 2021). As microorganisms shift from a free-living planktonic existence to a sessile, EPS-associated lifestyle, they commonly suppress flagellar gene expression and simultaneously activate genes governing extracellular polymeric substance (EPS)

https://doi.org/10.5194/egusphere-2025-6516
Preprint. Discussion started: 6 January 2026

biosynthesis, two-component regulatory systems (TCS), global transcriptional regulators, and quorum sensing (QS) signaling pathways (Petrova & Sauer, 2012; Guttenplan et al., 2013; Dang & Lovell, 2016; Shang et al., 2021). The epimerase encoded by galE (EC 5.1.3.2) served as a critical catalyst in the biosynthesis of UDP-galactose (Frey, 1996), whereas rmlC (EC 5.1.3.13) and rmlD (EC 1.1.1.133) were indispensable for the production of dTDP-rhamnose (Giraud & Naismith, 2000). The availability of sugar nucleotide precursors represents a key determinant of EPS biosynthesis. Psl is characterized as a repeating pentasaccharide composed of D-mannose, D-glucose, and L-rhamnose, playing a key role in adherence to surfaces and biofilm architecture maintenance (Flemming & Wingender, 2010). Additionally, bacteria can sense subtle environmental changes (e.g., pH, Ga^{2+} and Mg^{2+}) through specific sensing systems, such as *PhoQ* (EC 2.7.13.3) (Groisman, 2001; Groisman et al., 2021). Although the addition of cation-containing minerals (Fig.5) stimulated bacterial growth and promotes early flagellar motility (Tables S2), the downregulation of *PhoQ* further suppresses the expression of flagellar-related genes and the production of c-di-GMP (Fig.10a) (Li et al., 2024).

Microbially regulated flocculation processes directly influence the transformation, transport, and fate of carbon in estuarine environments (Bauer et al., 2013). Our path analysis elucidated the direct links between bacterial abundance and DOC, POC, and floc structure (Fig.11), confirming that this DOC-to-POC transformation is the material basis for floc stabilization (Chin et al., 1998; Verdugo et al. 2004; He et al. 2016). The equilibrium of the MSD flocs observed in this study was attributable to the consistent total EPS content. Once carbon sources (DOC and polysaccharides) become depleted, it inhibited microbial growth and induced EPS degradation or diffusion (Schleheck et al., 2009; Maalej et al., 2017), thereby compromising flocculation. This situation found support in illite bioflocculation experiments during the bacterial stationary phase (fig S1-3). Thus, microbial control of carbon availability directly limits the long-term trajectory of flocculation (Kovárová-Kovar & Egli, 1998).

Path analysis indicated that metabolism feed back into water chemistry (Fig.11), thereby indirectly affecting sediment transport. By reshaping suspended sediment transport, microorganisms influence estuarine turbidity regimes (Shi et al., 2017), nutrient and pollutant fluxes and the efficiency of carbon burial (Jiao et al., 2010; Bauer et al., 2013; Nguyen et al., 2022). Larger, carbon-enriched bio-flocs are more likely to

https://doi.org/10.5194/egusphere-2025-6516
Preprint. Discussion started: 6 January 2026

be exported offshore or deposited in carbon-rich estuarine sinks, strengthening the role of estuaries as hotspots for carbon cycling. These processes are particularly relevant under anthropogenic pressures such as eutrophication and climate-driven changes in river discharge (Harrison et al., 2008; Statham, 2012; Cloern et al., 2016; Wetz & Yoskowitz, 2013; Zhao et al., 2020), which may alter microbial community composition and activity (Mai et al., 2018; Wong et al., 2021). Our findings emphasize that sediment transport models and estuarine management strategies must explicitly account for microbial processes if they are to predict sediment and carbon fluxes under future environmental change.

5. Conclusions

By investigating the flocculation of the estuarine dominant strain *S. decontaminans* with montmorillonite under constant shear, this work establishes that microorganisms and EPS critically shape floc dynamics and structure, reveals the governing molecular mechanism, and directly links this process to the estuarine carbon cycle. The detailed results are summarized as followed:

1) Bio-mineral flocs exhibit significantly slower flocculation kinetics than purely inorganic systems in reaching equilibrium. At steady state, the aggregates in MSD achieve a mean diameter approximately four times larger, coupled with a distinctly lower fractal dimension of 1.43, possessing a larger, more porous, and more loosely structured morphology.
2) *S. decontaminans* and its EPS play a definitive role in both restructuring floc architecture and modifying the elemental composition of aggregates, elevating carbon content within a range of 7.4% to 53.9%;
3) Genes associated with flagellar structure and motility promote the initial adhesion of bacteria to mineral particles, whereas polysaccharide biosynthesis genes are essential for stabilizing floc structure;
4) The microbe-mediated flocculation process actively drives the conversion of DOC into POC and significantly alters key water chemistry parameters, including turbidity, pH, and zeta potential, thereby exerting a profound influence on biogeochemical processes.

https://doi.org/10.5194/egusphere-2025-6516
Preprint. Discussion started: 6 January 2026

Acknowledgements

This research was funded by the National Natural Science Foundation of China (42476155, 12411530095 and 42076173), and was also greatly supported by the Innovation Group Project of Southern Marine Science and Engineering Guangdong Laboratory (Zhuhai) (311021004).

References

Anvari-Yazdi, F., Tahermanesh, K., Joghataei, M. T., Tavangar, S. M., Moradi, F., Kashi, A., et al. (2014). How to prepare biological samples and live tissues for scanning electron microscopy (SEM). Galen Medical Journal, 3. 63-80.

Bauer, J. E., Cai, W. J., Raymond, P. A., Bianchi, T. S., Hopkinson, C. S., & Regnier, P. A. (2013). The changing carbon cycle of the coastal ocean. Nature, 504(7478), 61-70.

Baumas, C., & Bizic, M. (2024). A focus on different types of organic matter particles and their significance in the open ocean carbon cycle. Progress in Oceanography, 224, 103233.

Belas, R. (2014). Biofilms, flagella, and mechanosensing of surfaces by bacteria. Trends in microbiology, 22(9), 517-527.

Berne, C., Ellison, C. K., Ducret, A., & Brun, Y. V. (2018). Bacterial adhesion at the single-cell level. Nature Reviews Microbiology, 16(10), 616-627.

Burchard, H., Schuttelaars, H. M., & Ralston, D. K. (2018). Sediment trapping in estuaries. Annual review of marine science, 10(1), 371-395.

Burd, A. B., & Jackson, G. A. Particle aggregation. Annual Review of Marine Science, 2009, 1, 65-90.

Callahan, B. J., McMurdie, P. J., & Holmes, S. P. (2016). DADA2: high-resolution sample inference from Illumina amplicon data. Nature Methods, 13(7), 581-583.

Chapalain, M., Verney, R., Fettweis, M., Jacquet, M., Le Berre, D., & Le Hir, P. (2019). Investigating suspended particulate matter in coastal waters using the fractal theory. Ocean Dynamics, 69(1), 59-81.

Chen, Q., Ran, F., Wei, Q., Zheng, X., Zhao, M., Liu, S., ... & Fan, C. (2024). A review on dewatering of dredged sediment in water bodies by flocculation processes. Water, Air, & Soil Pollution, 235(1), 67.

Chin, W. C., Orellana, M. V., & Verdugo, P. (1998). Spontaneous assembly of marine

https://doi.org/10.5194/egusphere-2025-6516
Preprint. Discussion started: 6 January 2026

dissolved organic matter into polymer gels. Nature, 391(6667), 568-572.

Cloern, J. E., Abreu, P. C., Carstensen, J., Chauvaud, L., Elmgren, R., Grall, J., ... & Yin, K. (2016). Human activities and climate variability drive fast-paced change across the world's estuarine–coastal ecosystems. Global change biology, 22(2), 513-529.

Cox, J. R., Lingbeek, J., Weisscher, S. A. H., & Kleinhans, M. G. (2022). Effects of sea-level rise on dredging and dredged estuary morphology. Journal of Geophysical Research: Earth Surface, 127(10), e2022JF006790.

Cui, Z., Huang, L., Fang, H., Han, D., & Bombardelli, F. (2023). Exploring cohesive sediment flocculation with surface heterogeneity: a theoretical lagrangian-type flocculation model. Water Resources Research, 59(11), e2022WR034374.

Dang, H., & Lovell, C. R. (2016). Microbial surface colonization and biofilm development in marine environments. Microbiology and molecular biology reviews, 80(1), 91-138.

Dar, D., Dar, N., Cai, L., & Newman, D. K. (2021). Spatial transcriptomics of planktonic and sessile bacterial populations at single-cell resolution. Science, 373(6556), eabi4882.

Decho, A. W., & Gutierrez, T. (2017). Microbial extracellular polymeric substances (EPSs) in ocean systems. Front Microbiol 8: 922.

Deng, Z., He, Q., Manning, A. J., & Chassagne, C. (2023). A laboratory study on the behavior of estuarine sediment flocculation as function of salinity, EPS and living algae. Marine Geology, 459, 107029.

Deng, Z., Huang, D., He, Q., & Chassagne, C. (2022). Review of the action of organic matter on mineral sediment flocculation. Frontiers in Earth Science, 10, 965919.

Droppo, I. G. (2001). Rethinking what constitutes suspended sediment. Hydrological Processes, 15(9), 1551-1564.

DuBois, M., Gilles, K. A., Hamilton, J. K., Rebers, P. A., & Smith, F. (1956). Colorimetric method for determination of sugars and related substances. Analytical chemistry, 28(3), 350-356.

Fettweis, M., Schartau, M., Desmit, X., Lee, B. J., Terseleer, N., Van der Zande, D., ... & Riethmüller, R. (2022). Organic matter composition of biomineral flocs and its influence on suspended particulate matter dynamics along a nearshore to offshore transect. Journal of Geophysical Research: Biogeosciences, 127(1),

https://doi.org/10.5194/egusphere-2025-6516
Preprint. Discussion started: 6 January 2026

e2021JG006332.

Flemming, H. C., & Wingender, J. (2010). The biofilm matrix. Nature reviews microbiology, 8(9), 623-633.

Frey, P. A. (1996). The Leloir pathway: a mechanistic imperative for three enzymes to change the stereochemical configuration of a single carbon in galactose. The FASEB Journal, 10(4), 461-470.

Gattuso, J. P., Frankignoulle, M., & Wollast, R. (1998). Carbon and carbonate metabolism in coastal aquatic ecosystems. Annual Review of Ecology and Systematics, 29(1), 405-434.

Gerbersdorf, S. U., & Wieprecht, S. (2015). Biostabilization of cohesive sediments: revisiting the role of abiotic conditions, physiology and diversity of microbes, polymeric secretion, and biofilm architecture. Geobiology, 13(1), 68-97.

Giraud, M. F., & Naismith, J. H. (2000). The rhamnose pathway. Current opinion in structural biology, 10(6), 687-696.

Groisman, E. A. (2001). The pleiotropic two-component regulatory system PhoP-PhoQ. Journal of bacteriology, 183(6), 1835-1842.

Groisman, E. A., Duprey, A., & Choi, J. (2021). How the PhoP/PhoQ system controls virulence and Mg2+ homeostasis: lessons in signal transduction, pathogenesis, physiology, and evolution. Microbiology and Molecular Biology Reviews, 85(3), 10-1128.

Guo, C., Manning, A. J., Bass, S., Guo, L., & He, Q. (2021). A quantitative lab examination of floc fractal property considering influences of turbulence, salinity and sediment concentration. Journal of Hydrology, 601, 126574.

Guo, J., Qiu, X., Xie, Y. G., Hua, Z. S., & Wang, Y. (2024). Regulation of intracellular process by two-component systems: Exploring the mechanism of plasmid-mediated conjugative transfer. Water Research, 259, 121855.

Guttenplan, S. B., & Kearns, D. B. (2013). Regulation of flagellar motility during biofilm formation. FEMS microbiology reviews, 37(6), 849-871.

Harrison, P. J., Yin, K., Lee, J. H. W., Gan, J., & Liu, H. (2008).Physical–biological coupling in the Pearl River Estuary. Continental Shelf Research, 28(12), 1405-1415.

He, B., Dai, M., Zhai, W., Wang, L., Wang, K., Chen, J., ... & Xu, Y. (2010). Distribution, degradation and dynamics of dissolved organic carbon and its major

https://doi.org/10.5194/egusphere-2025-6516
Preprint. Discussion started: 6 January 2026

compound classes in the Pearl River estuary, China. Marine Chemistry, 119(1-4), 52-64.

He, K., Shi, X., Tao, Z., Hu, X., Sun, L., Wang, R., ... & Lei, P. (2024). Genomic and genomic and transcriptomic analyses identify two key glycosyltransferase genes alhH and alhK of exopolysaccharide biosynthesis in Pantoea alhagi NX-11. Microorganisms, 12(10), 2016.

He, W., Chen, M., Schlautman, M. A., & Hur, J. (2016). Dynamic exchanges between DOM and POM pools in coastal and inland aquatic ecosystems: A review. Science of the Total Environment, 551, 415-428.

Ho, Q. N., Fettweis, M., Hur, J., Desmit, X., Kim, J. I., Jung, D. W., ... & Lee, B. J. (2022). Flocculation kinetics and mechanisms of microalgae-and clay-containing suspensions in different microalgal growth phases. Water Research, 226, 119300.

Jiao, N., Herndl, G. J., Hansell, D. A., Benner, R., Kattner, G., Wilhelm, S. W., ... & Azam, F. (2010). Microbial production of recalcitrant dissolved organic matter: long-term carbon storage in the global ocean. Nature Reviews Microbiology, 8(8), 593-599.

Jocher, G., Chaurasia, A., & Qiu, J. (2023). YOLOv8 by Ultralytics. https://github.com/ultralytics/ultralytics

Kovárová-Kovar, K., & Egli, T. (1998). Growth kinetics of suspended microbial cells: from single-substrate-controlled growth to mixed-substrate kinetics. Microbiology and molecular biology reviews, 62(3), 646-666.

Labille, J., Thomas, F., Milas, M., & Vanhaverbeke, C. (2005). Flocculation of colloidal clay by bacterial polysaccharides: effect of macromolecule charge and structure. Journal of colloid and interface science, 284(1), 149-156.

Lai, H., Fang, H., Huang, L., He, G., & Reible, D. (2018). A review on sediment bioflocculation: Dynamics, influencing factors and modeling. Science of the total environment, 642, 1184-1200.

Li, J., Salam, N., Wang, P., Chen, L., Jiao, J., Li, X., ... & Li, W. (2018). Discordance between resident and active bacterioplankton in free-living and particle-associated communities in estuary ecosystem. Microbial ecology, 76(3), 637-647.

Li, X., Zhang, X., Zhang, M., Luo, X., Zhang, T., Liu, X., ... & Zhang, Y. (2024). Environmental magnesium ion affects global gene expression, motility, biofilm formation and virulence of Vibrio parahaemolyticus. Biofilm, 7, 100194.

https://doi.org/10.5194/egusphere-2025-6516
Preprint. Discussion started: 6 January 2026

598 Li, Y., Guo, N., Yuan, K., Chen, B., Wang, J., Hua, M., ... & Yang, Y. (2023).
599 Variations in the concentration, source and flux of polycyclic aromatic
600 hydrocarbons in sediments of the Pearl River Estuary: Implications for
601 anthropogenic impacts. Science of the Total Environment, 862, 160870.
602 Lowry, O. H., Rosebrough, N. J., Farr, A. L., & Randall, R. J. (1951). Protein
603 measurement with the Folin phenol reagent. Journal of Biological Chemistry,
604 193(1), 265-275.
605 Maalej, H., Boisset, C., Hmidet, N., Colin-Morel, P., Buon, L., & Nasri, M. (2017).
606 Depolymerization of Pseudomonas stutzeri exopolysaccharide upon fermentation
607 as a promising production process of antibacterial compounds. Food chemistry,
608 227, 22-32.
609 Maggi, F. (2009). Biological flocculation of suspended particles in nutrient-rich
610 aqueous ecosystems. Journal of Hydrology, 376(1-2), 116-125.
611 Maggi, F. (2013). The settling velocity of mineral, biomineral, and biological particles
612 and aggregates in water. Journal of Geophysical Research: Oceans, 118(4), 2118-
613 2132.
614 Mai, Y. Z., Lai, Z. N., Li, X. H., Peng, S. Y., & Wang, C. (2018). Structural and
615 functional shifts of bacterioplanktonic communities associated with
616 spatiotemporal gradients in river outlets of the subtropical Pearl River Estuary,
617 South China. Marine Pollution Bulletin, 136, 309-321.
618 Mari, X., Passow, U., Migon, C., Burd, A. B., & Legendre, L. (2017). Transparent
619 exopolymer particles: Effects on carbon cycling in the ocean. Progress in
620 Oceanography, 151, 13-37.
621 Mietta, F., Chassagne, C., Manning, A. J., & Winterwerp, J. C. (2009). Influence of
622 shear rate, organic matter content, pH and salinity on mud flocculation. Ocean
623 Dynamics, 59(5), 751-763.
624 Moruzzi, R. B., de Oliveira, A. L., da Conceição, F. T., Gregory, J., & Campos, L. C.
625 (2017). Fractal dimension of large aggregates under different flocculation
626 conditions. Science of the Total Environment, 609, 807-814.
627 Mulet, M., Gomila, M., Lalucat, J., Bosch, R., Rossello-Mora, R., & García-Valdés, E.
628 (2023). Stutzerimonas decontaminans sp. nov. isolated from marine polluted
629 sediments. Systematic and Applied Microbiology, 46(2), 126400.
630 Nguyen, T. H., Tang, F. H., & Maggi, F. (2017). Optical measurement of cell

https://doi.org/10.5194/egusphere-2025-6516
Preprint. Discussion started: 6 January 2026

631 colonization patterns on individual suspended sediment aggregates. Journal of
632 Geophysical Research: Earth Surface, 122(10), 1794-1807.
633 Nguyen, T. H., Tang, F. H., & Maggi, F. (2018). Micro food web networks on
634 suspended sediment. Science of the Total Environment, 643, 1387-1399.
635 Nguyen, T. T., Zakem, E. J., Ebrahimi, A., Schwartzman, J., Caglar, T., Amarnath,
636 K., ... & Levine, N. M. (2022). Microbes contribute to setting the ocean carbon
637 flux by altering the fate of sinking particulates. Nature communications, 13(1),
638 1657.
639 O'Toole, G. A., & Kolter, R. (1998). Flagellar and twitching motility are necessary for
640 Pseudomonas aeruginosa biofilm development. Molecular microbiology, 30(2),
641 295-304.
642 Passow, U. (2002). Transparent exopolymer particles (TEP) in aquatic environments.
643 Progress in oceanography, 55(3-4), 287-333.
644 Passow, U., & De La Rocha, C. L. (2006). Accumulation of mineral ballast on organic
645 aggregates. Global Biogeochemical Cycles, 20(1).
646 Petrova, O. E., & Sauer, K. (2012). Sticky situations: key components that control
647 bacterial surface attachment. Journal of Bacteriology, 194(10), 2413–2425.
648 Rana, S., & Upadhyay, L. S. B. (2020). Microbial exopolysaccharides: Synthesis
649 pathways, types and their commercial applications. International journal of
650 biological macromolecules, 157, 577-583.
651 Schleheck, D., Barraud, N., Klebensberger, J., Webb, J. S., McDougald, D., Rice, S. A.,
652 & Kjelleberg, S. (2009). Pseudomonas aeruginosa PAO1 preferentially grows as
653 aggregates in liquid batch cultures and disperses upon starvation. PloS one, 4(5),
654 e5513.
655 Schmid, J., Sieber, V., & Rehm, B. (2015). Bacterial exopolysaccharides: biosynthesis
656 pathways and engineering strategies. Frontiers in microbiology, 6, 496.
657 Shang, L., Yan, Y., Zhan, Y., Ke, X., Shao, Y., Liu, Y., ... & Lin, M. (2021). A
658 regulatory network involving Rpo, Gac and Rsm for nitrogen-fixing biofilm
659 formation by Pseudomonas stutzeri. npj Biofilms and Microbiomes, 7(1), 54.
660 Shen, X., Toorman, E. A., Lee, B. J., & Fettweis, M. (2019). An approach to modeling
661 biofilm growth during the flocculation of suspended cohesive sediments. Journal
662 of Geophysical Research: Oceans, 124(6), 4098-4116.
663 Shi, Z., Xu, J., Huang, X., Zhang, X., Jiang, Z., Ye, F., & Liang, X. (2017). Relationship

https://doi.org/10.5194/egusphere-2025-6516
Preprint. Discussion started: 6 January 2026

664 between nutrients and plankton biomass in the turbidity maximum zone of the
665 Pearl River Estuary. Journal of Environmental Sciences, 57, 72-84.
666 Shukla, A., Mehta, K., Parmar, J., Pandya, J., & Saraf, M. (2019). Depicting the
667 exemplary knowledge of microbial exopolysaccharides in a nutshell. European
668 Polymer Journal, 119, 298-310.
669 Statham, P. J. (2012). Nutrients in estuaries—An overview and the potential impacts of
670 climate change. Science of the total environment, 434, 213-227.
671 Sun, X., & Zhang, J. (2021). Bacterial exopolysaccharides: Chemical structures, gene
672 clusters and genetic engineering. International Journal of Biological
673 Macromolecules, 173, 481-490.
674 Tang, F. H., & Maggi, F. (2016). A mesocosm experiment of suspended particulate
675 matter dynamics in nutrient-and biomass-affected waters. Water Research, 89, 76-
676 86.
677 Tkacz, A., Hortala, M., & Poole, P. S. (2018). Absolute quantitation of microbiota
678 abundance in environmental samples. Microbiome, 6(1), 110.
679 Tran, D., Kuprenas, R., & Strom, K. (2018). How do changes in suspended sediment
680 concentration alone influence the size of mud flocs under steady turbulent
681 shearing?. Continental Shelf Research, 158, 1-14.
682 Turner, A., & Millward, G. E. (2002). Suspended particles: their role in estuarine
683 biogeochemical cycles. Estuarine, Coastal and Shelf Science, 55(6), 857-883.
684 Verdugo, P., Alldredge, A. L., Azam, F., Kirchman, D. L., Passow, U., & Santschi, P.
685 H. (2004). The oceanic gel phase: a bridge in the DOM–POM continuum. Marine
686 chemistry, 92(1-4), 67-85.
687 Wadhwa, N., & Berg, H. C. (2022). Bacterial motility: machinery and mechanisms.
688 Nature reviews microbiology, 20(3), 161-173.
689 Walshire, L. A., Zhang, H., Nick, Z. H., Breland, B. R., Runge, K. A., & Han, F. X.
690 (2024). Modification of surface properties of clay minerals with
691 exopolysaccharides from rhizobium tropici. ACS Earth and Space Chemistry, 8(1),
692 137-147.
693 Wetz, M. S., & Yoskowitz, D. W. (2013). An ‘extreme’future for estuaries? Effects of
694 extreme climatic events on estuarine water quality and ecology. Marine Pollution
695 Bulletin, 69(1-2), 7-18.
696 Winterwerp, J. C. (1998). A simple model for turbulence induced flocculation of

https://doi.org/10.5194/egusphere-2025-6516
Preprint. Discussion started: 6 January 2026

cohesive sediment. Journal of hydraulic research, 36(3), 309-326.

Wong, G. C., Antani, J. D., Lele, P. P., Chen, J., Nan, B., Kühn, M. J., ... & Dunkel, J. (2021). Roadmap on emerging concepts in the physical biology of bacterial biofilms: from surface sensing to community formation. Physical biology, 18(5), 051501.

Wu, S., Zheng, R., Sha, Z., & Sun, C. (2017). Genome sequence of Pseudomonas stutzeri 273 and identification of the exopolysaccharide EPS273 biosynthesis locus. Marine drugs, 15(7), 218.

Ye, L., Wu, J., Huang, M., & Yan, J. (2023). The role of suspended extracellular polymeric substance (EPS) on equilibrium flocculation of clay minerals in high salinity water. Water Research, 244, 120451.

Zhao, K., Pomes, F., Vowinckel, B., Hsu, T. J., Bai, B., & Meiburg, E. (2021). Flocculation of suspended cohesive particles in homogeneous isotropic turbulence. Journal of Fluid Mechanics, 921, A17.

Zhao, Y., Liu, J., Uthaipan, K., Song, X., Xu, Y., He, B., ... & Dai, M. (2020). Dynamics of inorganic carbon and pH in a large subtropical continental shelf system: Interaction between eutrophication, hypoxia, and ocean acidification. Limnology and Oceanography, 65(6), 1359-1379.

Zhu, L., Zhang, H., Guo, L., Huang, W., & Gong, W. (2021). Estimation of riverine sediment fate and transport timescales in a wide estuary with multiple sources. Journal of Marine Systems, 214, 103488.

https://doi.org/10.5194/egusphere-2025-6516
Preprint. Discussion started: 6 January 2026

720 **Figures list and captions:**

721

722

723

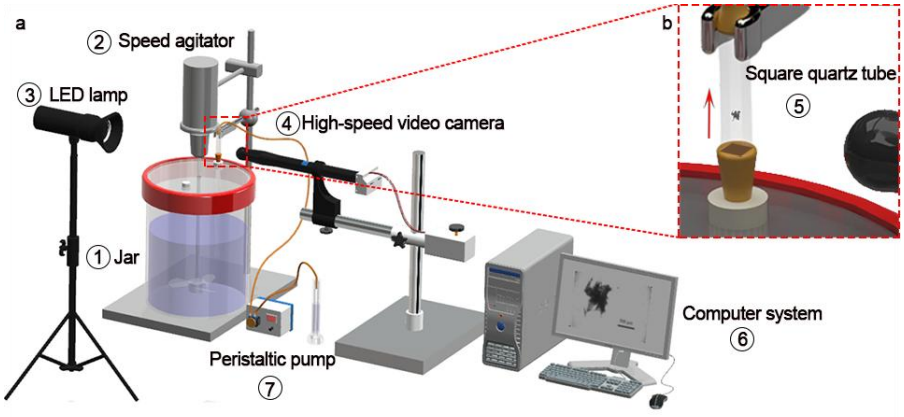

724 **Figure 1.** (a) Schematic of the laboratory experimental setup. The main components
725 are: (1) jar, (2) LED lamp, (3) variable-speed agitator, (4) high-speed digital camera,
726 (5) square quartz tube, (6) peristaltic pump, and (7) computer system. (b) Detailed
727 view of the square quartz tube, showing the "shooting point" location. The red arrow
728 indicates the flow direction of the suspension.

729

730

https://doi.org/10.5194/egusphere-2025-6516
Preprint. Discussion started: 6 January 2026

731

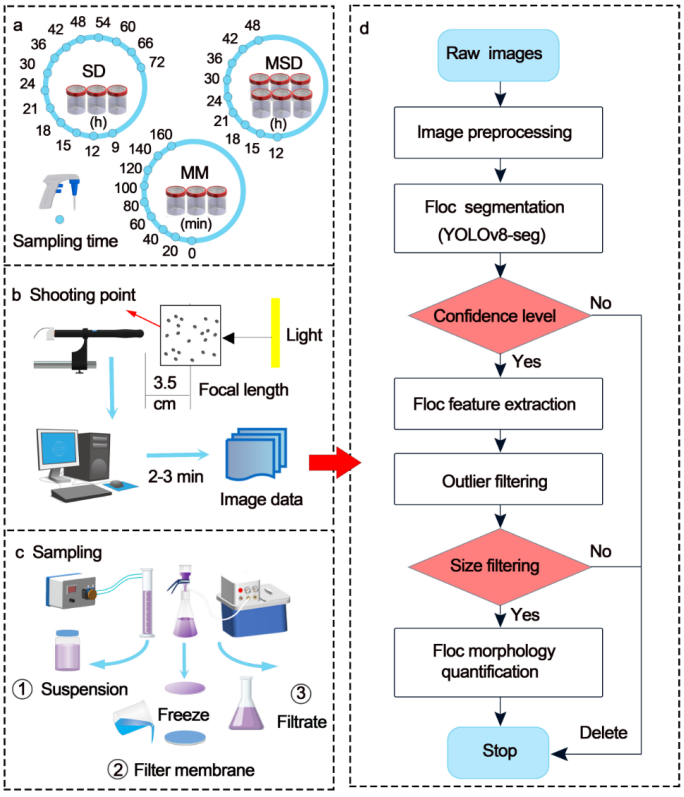

732 **Figure 2.** The main experimental workflow includes (a) sampling time, (b) image
733 acquisition, (c) sample collection and (d) image analysis. (The blue dots along the
734 circles represent the sampling timepoints for the SD (9-72 h), and MSD (12-48 h),
735 MM (0-160 min) treatments. A high-speed digital camera equipped with a fixed focal
736 length of approximately 3.5 cm was employed for a 2-3 min imaging. At each
737 sampling time, particle suspensions, filter membranes (flash-frozen in liquid N_2), and
738 filtrates were collected for SD and MSD.)
739

https://doi.org/10.5194/egusphere-2025-6516
Preprint. Discussion started: 6 January 2026

740

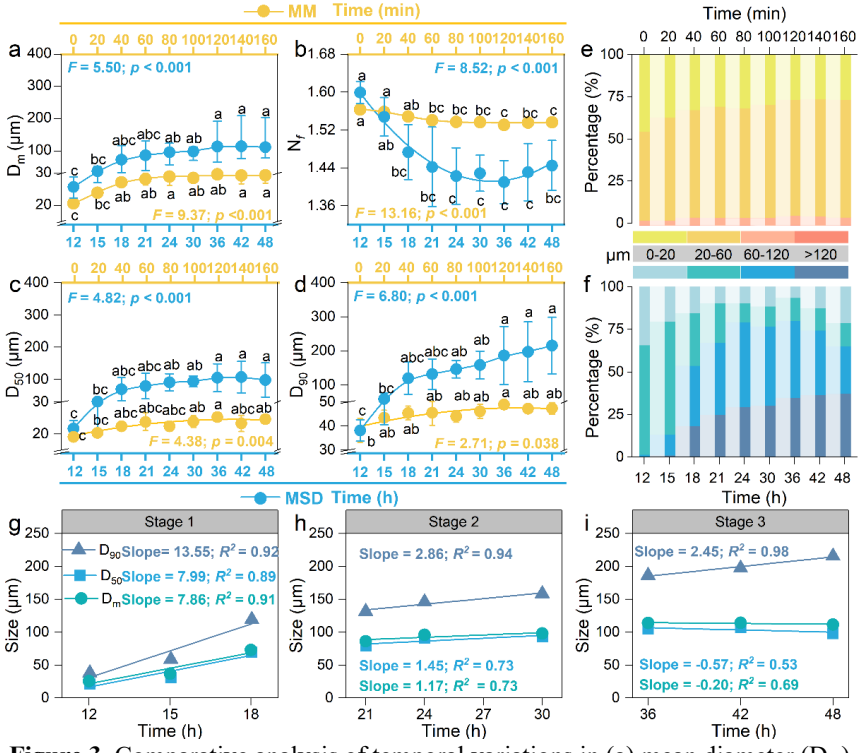

741 **Figure 3.** Comparative analysis of temporal variations in (a) mean diameter (D_m), (b)
742 fractal dimension (N_f), (c) D_{50}, (d) D_{90} between MM and MSD. Temporal variations
743 in size-class distributions in (e) MM and (f) MSD, respectively. Stage-resolved floc
744 size dynamics and slope transitions in MSD in (g) phase one (12-18 h), (h) phase two
745 (21-30 h), and (i) phase three (36-48 h). (MM: Montmorillonite mineral system;
746 MSD: Montmorillonite mineral and *S. decontaminans* mixed system. Different
747 lowercase letters represented significant differences between treatments ($P < 0.05$) by
748 HSD test.)
749
750

https://doi.org/10.5194/egusphere-2025-6516
Preprint. Discussion started: 6 January 2026

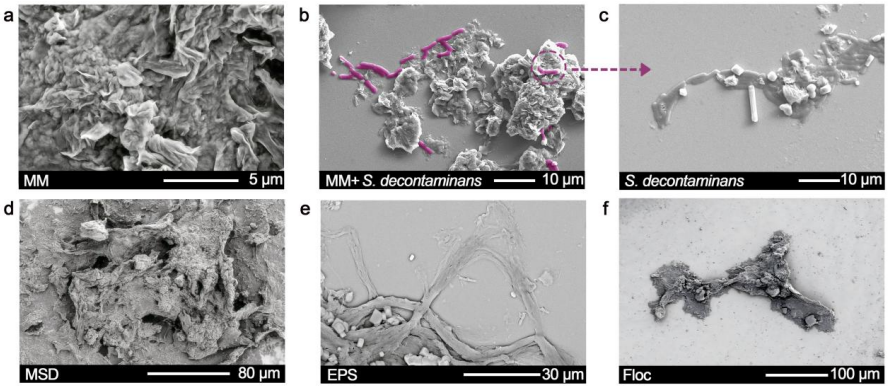

Figure 4. Scanning electron micrographs of samples in MM and MSD. (a) Mineral surface structure in MM, (b) Mineral particles and microorganisms in MSD, (c) *S. decontaminans*,(d) Mixing sample including mineral, microorganisms and EPS in MSD, (e) EPS, (f) Floc of MSD. (MM: Montmorillonite mineral system, MSD: Montmorillonite mineral and *S. decontaminans* mixed system.)

https://doi.org/10.5194/egusphere-2025-6516
Preprint. Discussion started: 6 January 2026

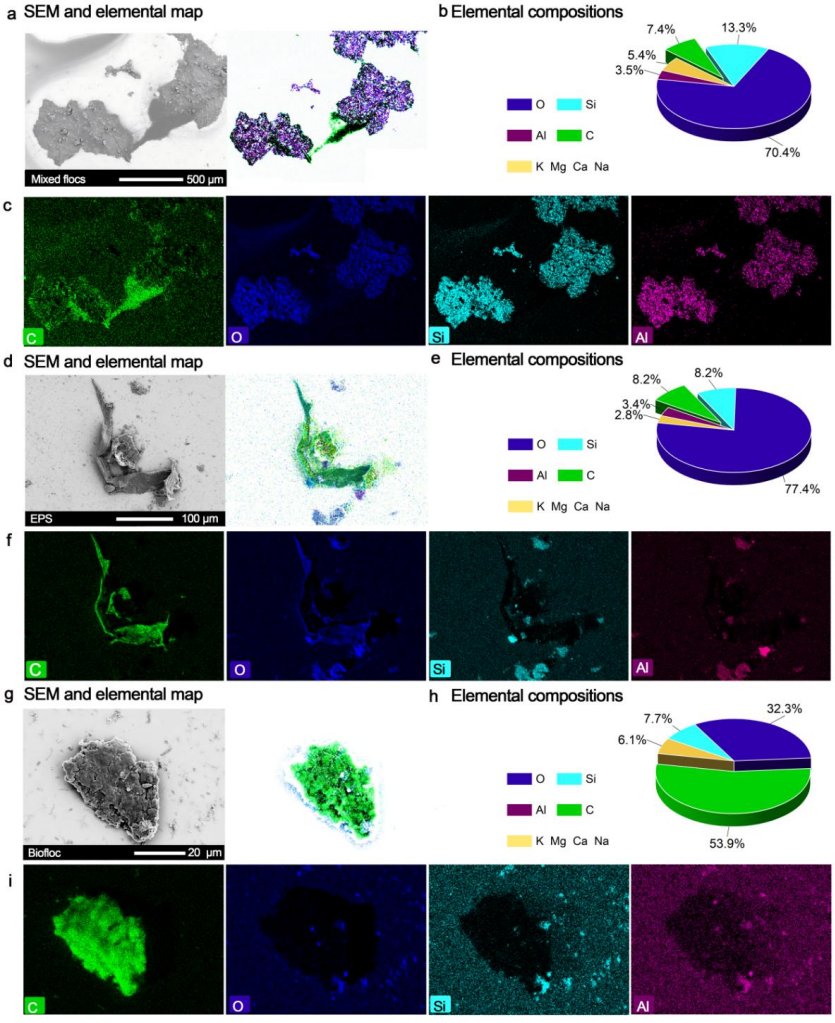

758 **Figure 5**. SEM characterization and elemental analysis of floc components in
759 MSD:SEM images, elemental compositions and maps (C, O, Si, Al) for mixed flocs
760 (a-c), EPS (d-f), and bio-floc (g-i).
761

https://doi.org/10.5194/egusphere-2025-6516
Preprint. Discussion started: 6 January 2026

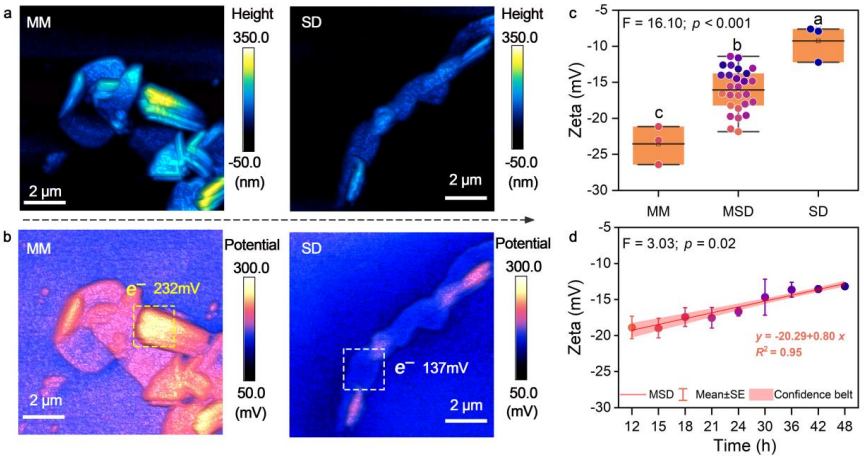

Figure 6. Atomic force microscope (AFM) images of MM and SD's (a) surface roughness and (b) potential mapping, (c) Comparison of Zeta-potential among MM, MSD and SD, and (d) temporal characters of Zeta-potential in MSD. (MM: Montmorillonite mineral system, SD: a pure culture of *S. decontaminans*, MSD: Montmorillonite mineral and *S. decontaminans* mixed system. Different lowercase letters represented significant differences between treatments ($P < 0.05$) by HSD test.)

https://doi.org/10.5194/egusphere-2025-6516
Preprint. Discussion started: 6 January 2026

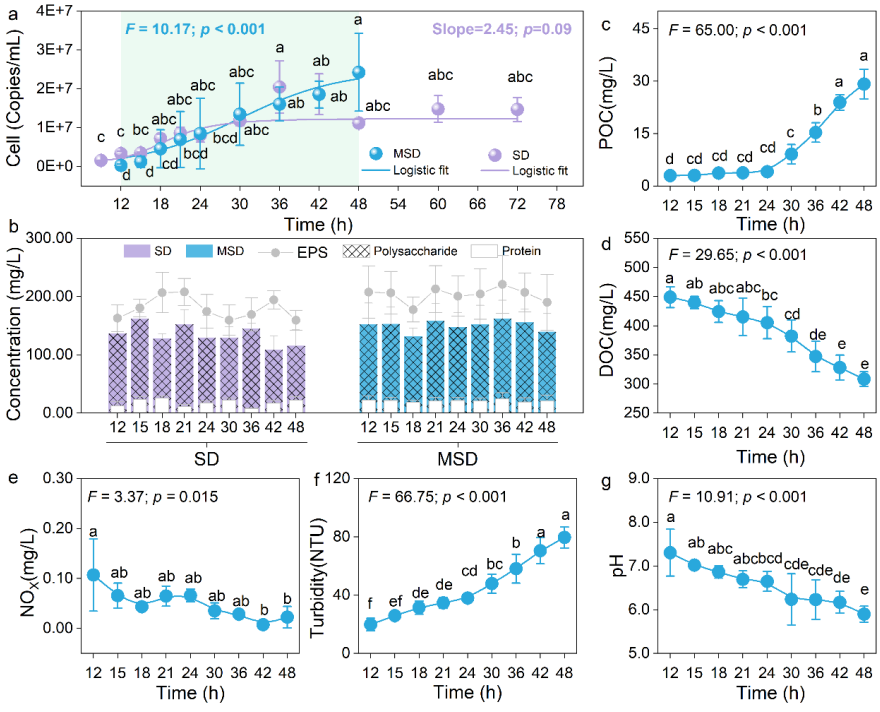

Figure 7. Temporal variations of (a) bacteria abundance, (b) EPS (gray line), polysaccharide (patterned boxes), and protein (white boxes) concentrations in MSD (blue) and SD (purple), and (c) particulate organic carbon (POC), (d) dissolved organic carbon (DOC), (e) $NO_x = NO_2^- + NO_3^- + NH_4^+$, (f) turbidity (NTU), (g) pH value in MSD. (MSD: Montmorillonite mineral and *S. decontaminans* mixed system. Different lowercase letters represented significant differences between treatments ($P < 0.05$) by HSD test.)

https://doi.org/10.5194/egusphere-2025-6516
Preprint. Discussion started: 6 January 2026

778

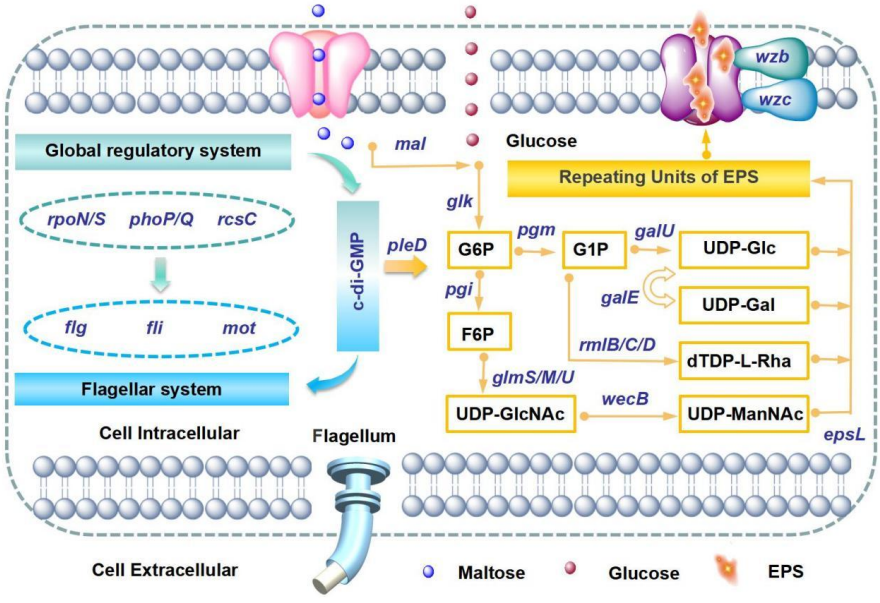

779 **Figure 8.** Gene regulatory network of *S. decontaminans* implicated in EPS regulation.
780 The depicted systems include: (1) global regulatory system (*rpoN/S, phoP/Q, rcsC*)
781 that activate cell motility and polysaccharide production; (2) flagellar system (flg, fli,
782 mot) that mediate bacterial motility; (3) polysaccharide system (e.g., *pleD, mal, glk,*
783 *pgi, pgm, galU, galE, rmlB/C/D, glmS/M/U, wecB, epsL*) essential for EPS assembly
784 and export. (F6P: Fructose-6-phosphate, G1P: Glucose-1-phosphate, UDP-GlcNAc:
785 Uridine diphosphate N-acetylglucosamine, UDP-Glc: Uridine diphosphate glucose,
786 UDP-Gal：Uridine diphosphate galactose, dTDP-L-Rha: Deoxythymidine
787 diphosphate L-rhamnose, UDP-ManNAc: Uridine diphosphate N-
788 acetylmannosamine).
789

https://doi.org/10.5194/egusphere-2025-6516
Preprint. Discussion started: 6 January 2026

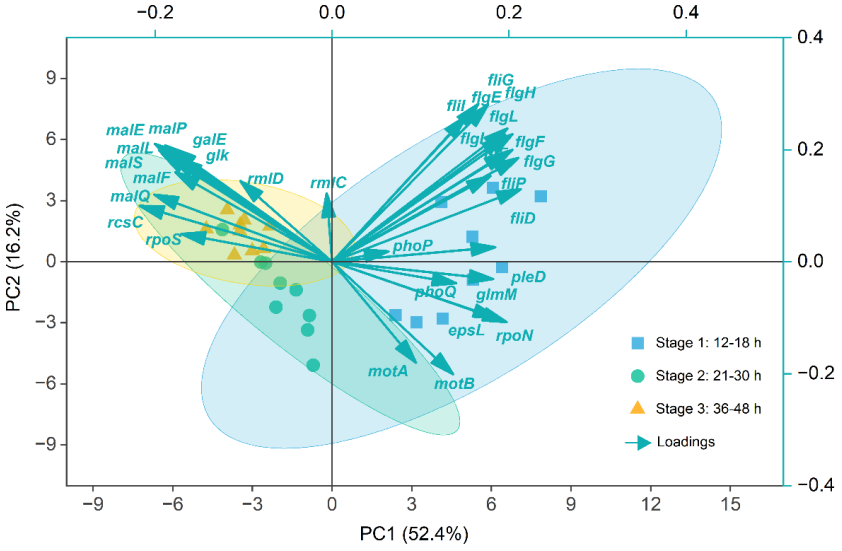

Figure 9. PCA of expressed genes and the differentially expressed genes across flocculation Stages one (12-18 h), two (21-30 h), and there (36-48 h). (All gene data were log2-transformed.)

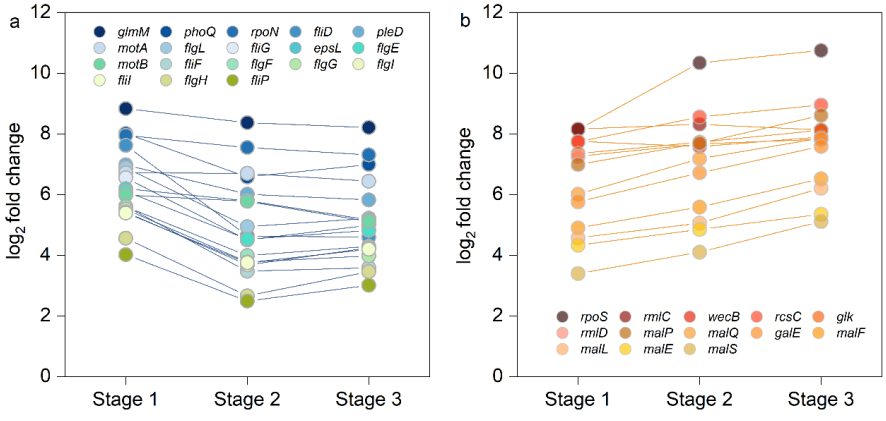

Figure 10. Dynamic expression changes of (a) up- and (b) down-regulated genes across flocculation Stages one (12-18 h), two (21-30 h), and there (36-48 h).

https://doi.org/10.5194/egusphere-2025-6516
Preprint. Discussion started: 6 January 2026

800

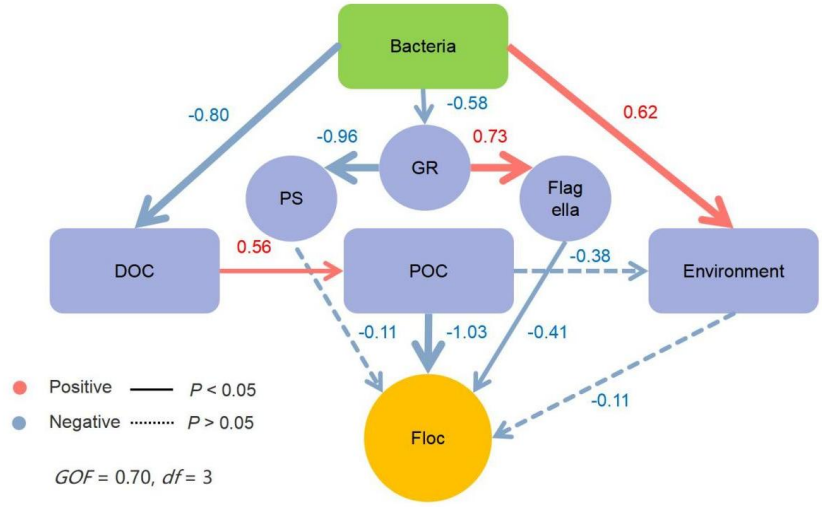

801 **Figure 11.** Structural equation model linking bacteria, gene, environmental response
802 and floc structures in MSD. (Numbers beside arrows indicated standardized
803 coefficients. Solid lines indicated significant relationships. The red lines and arrows
804 indicated positive effects. Bacteria, copy number of the bacterial cells; GR, Global
805 regulatory system, PS, polysaccharide system, Flagella, Flagellar system, POC,
806 particulate organic carbon, DOC, dissolved organic carbon, Environment included
807 pH, turbidity, NOX-, Zeta, Floc structure included D_m, D_{50}, D_{90}, N_f.)
808

https://doi.org/10.5194/egusphere-2025-6516
Preprint. Discussion started: 6 January 2026

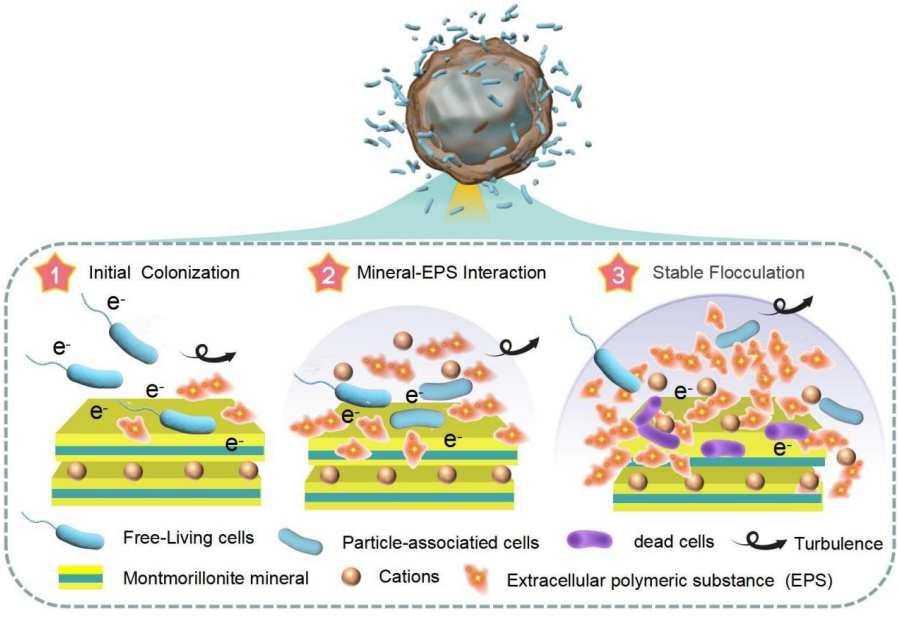

Figure 12. A three-stage conceptual framework for microbial modulation of flocculation.